nature chemistry

Article

https://doi.org/10.1038/s41557-025-01999-2

Developing design guidelines for controlling charge transport in DNA

Received: 18 November 2024

Accepted: 17 October 2025

Published online: 18 November 2025

Check for updates

Zahra Aminiranjbar[1,5], Caglanaz Akin Gultakti[2,3,5], Amy Zhang[1], Ersin Emre Oren[2,3] ✉ & Joshua Hihath[1,4] ✉

Conceptual frameworks that describe the electronic structure of molecules are an integral part of understanding chemical structures and reaction mechanisms and designing organic compounds. Here we develop a preliminary set of design guidelines for controlling the electronic structure of DNA. Recent work indicates that charge delocalization occurs over several bases and results in coherence lengths greater than a single base pair. To examine the interactions between bases and their effects on delocalization, this study investigates the influence of nearest-neighbour base pair interactions on the charge transport properties of DNA duplexes that are predominantly composed of guanine–cytosine base pairs. Results show that, by manipulating the sequence, the conductance can be substantially modified without altering the molecular composition. The electronic density of states are then analysed to deduce a set of design guidelines aimed at maintaining high conductance values in long duplexes. Utilizing these rules, we demonstrate that 20-base-pair DNA sequences can exhibit conductance values surpassing $1 \times 10^{-3} G_0$.

Understanding and eventually engineering coherence and state lifetimes in soft matter and nanoscale systems is critical to improving our understanding of a variety of biological and chemical systems[1], as well as to the long-term development of soft-matter quantum systems[2], organic photovoltaics[3] and molecular electronics[4,5]. Relatively rigid, large-scale, carbon-based, π-delocalized systems such as carbon nanotubes and graphene are well known to exhibit stable band structures and maintain charge coherence over long distances even at room temperature. However, many organic systems lack long-range order and electron delocalization[6,7]. They can also undergo rapid structural fluctuations and coupling to the environment, which drastically reduces charge coherence lengths and lifetimes. Here, we aim to demonstrate that, despite these interactions with warm and wet real-world environments, the electronic structure of floppy, weakly interacting, extended systems can be reliably controlled using a set of conceptually simple chemical design guidelines by using DNA as a model system.

Obtaining consistent electrical properties from DNA-based molecular wires has posed challenges. A wide range of conductance values and transport mechanisms were initially reported[8–14], demonstrating the importance of environmental and structural control when examining DNA's electronic properties[15]. More recent work in aqueous environments has provided robust insights into the charge transport properties of DNA over short length scales (<10 nm) (refs. 16–23). In particular, single-molecule break junction approaches have enabled a range of measurements with reproducible conductance values for short double-stranded DNA sequences[16–20,24–27]. These studies reveal that coherent tunnelling and incoherent hopping can both occur in DNA[16,21,22,25,28–31]. In a guanine–cytosine (G–C) base pair (bp) stack, charge movement occurs primarily through hopping, resulting in a conductance with a linear length dependence[32], while for adenine–thymine (A–T), tunnelling predominantly controls the transport over short distances[33,34]. More recently it has been shown that the coherence length

[1]Department of Electrical and Computer Engineering, University of California Davis, Davis, CA, USA. [2]Bionanodesign Laboratory, Department of Biomedical Engineering, TOBB University of Economics and Technology, Ankara, Turkey. [3]Department of Materials Science and Nanotechnology Engineering, TOBB University of Economics and Technology, Ankara, Turkey. [4]Center for Bioelectronics and Biosensors, School of Electrical, Computer, and Energy Engineering, Arizona State University, Phoenix, AZ, USA. [5]These authors contributed equally: Zahra Aminiranjbar, Caglanaz Akin Gultakti. ✉e-mail: eeoren@gmail.com; jhihath@asu.edu

https://doi.org/10.1038/s41557-025-01999-2

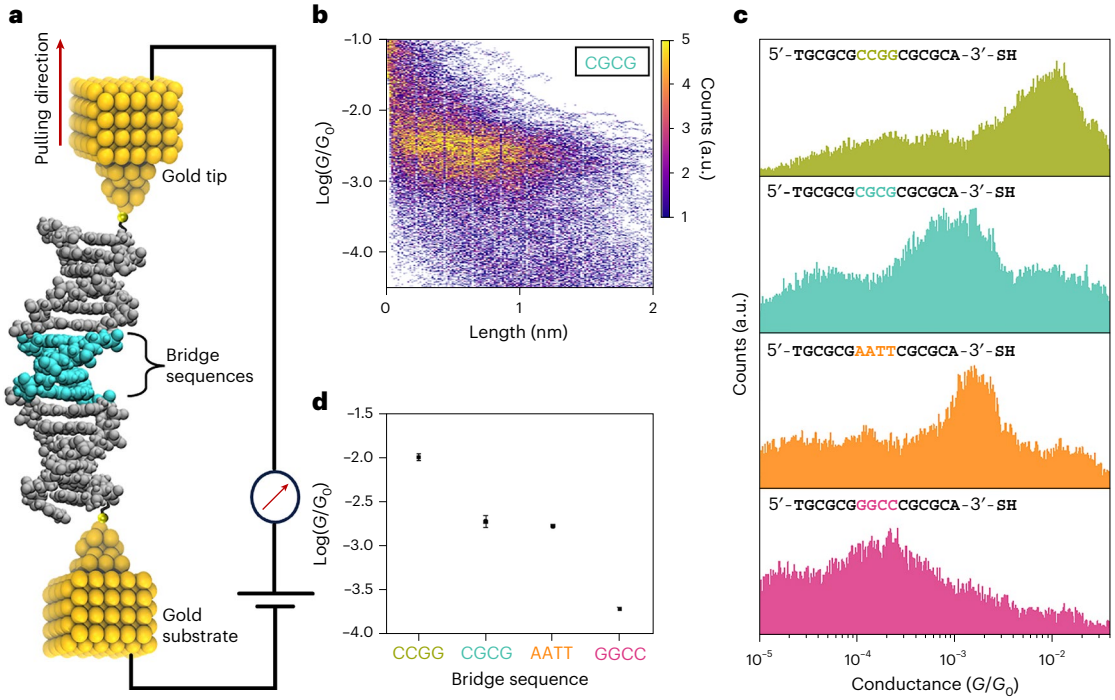

Fig. 1 | Break junction experiments on 16-bp molecules. a, An illustration of a STM-BJ with a DNA molecule bridging between the gold tip and the substrate. **b**, 2D histogram of conductance versus distance traces obtained from STM-BJ experiments on CGCG. **c**, Histograms illustrating the conductance distributions for the four DNA sequences. **d**, A scatter plot depicting the extracted conductance values derived from the histogram analysis with the error bars representing the standard error of the mean ($N = 4$).

of charge carriers in G–C systems can be much longer than a single base pair, suggesting that this simple hopping model is insufficient to capture the complex transport behaviour and, as such, a coherence corrected hopping model has been invoked[2,17]. Along these lines, it has been shown that stacks of guanines along one strand in DNA yield charge delocalization over several base pairs, resulting in much longer-range coherence than was initially predicted in a hopping-based system[17].

These studies underscore the important role that nearest-neighbor base pair (NNBP) interactions play in dictating the transport properties of DNA, and suggest it is possible to control the transport behaviour by modifying the sequence without modifying the overall DNA composition. This possibility is in stark contrast to cases where charge is localized on a single base at a time while moving through the stack. In such a case, the base order does not matter, and all G–C systems of a certain length should have the same conductance value. Thus, understanding the role of nearest neighbours is critically important for the design of DNA-based nanoelectronic sensors[35–39].

In this study, we build on these previous observations[17] by directly investigating the role of NNBP interactions on the conductance and density of states (DoS) of G–C-based DNA sequences. Our analysis centres on understanding the influence neighbouring bases have on the distribution of the DoS in both spatial and energy domains, which provides insights into charge delocalization and the corresponding coherence length. For this study, we initially employ a series of 16 base sequences with identical composition and focus on controlling the energy state distribution and NNBP interactions by modifying the four central bases. Circular dichroism (CD) and molecular dynamics (MD) analysis confirm that the selected sequences maintain their conformation in solution at room temperature. Conductance measurements are performed using the scanning tunnelling microscope break junction (STM-BJ) technique in solution phase to examine how the sequence affects DNA conductance. By further examining the energy level density and distribution using density functional theory (DFT), we establish a set of preliminary design guidelines for constructing longer DNA sequences. Finally, we utilize these guidelines to design the electronic structure of a series of 20-bp DNA sequence that have charge delocalized over several bases and exhibit high conductance values even at these length scales (~7 nm).

Results and discussion

In our initial investigation into the impact of NNBPs on charge transport in DNA, we utilized four DNA molecules with the sequence 5′-TGCGCG-XXXX-CGCGCA-3′-thiol C3, where 'XXXX' represents the bridge sequences that were used to study the effects of coupling on conductance. These selected DNA molecules were synthesized with a thiol linker at the 3′ end. They are self-complementary, but not fully periodic, and they spontaneously form DNA duplexes in solution, with thiols at either end to function as anchoring points for their attachment to gold electrodes.

We began with four bridge sequences (XXXX), namely, CCGG, GGCC, CGCG and AATT. Notably, both theoretical and experimental findings have demonstrated that G doublets (GG) and triplets (GGG) possess lower ionization potentials compared with a single G, indicating the coupling between the π-orbitals in these systems is sufficiently large to cause energy level splitting[23,29,40]. Incorporating this phenomenon into our design, we arranged adjacent G bases near the bridge in distinct orientations, enabling different electronic couplings and ionization potentials in the first three sequences. In addition, we note that long G–C-rich sequences are challenging to synthesize and purify[41], difficult to sequence[42] and are prone to form undesired secondary structures such as hairpins and G-quadruplexes[43,44], all of which can limit the utilization of such DNA sequences for applications[31]. Therefore, in the last sequence, AATT, we introduced A and T bases as a control for comparison and to provide design insights for practical longer DNA systems.

Conductance of 16-bp sequences

To measure the conductance of the DNA molecules, we employed the STM-BJ technique[27] (Fig. 1a and Methods). We collected thousands

https://doi.org/10.1038/s41557-025-01999-2

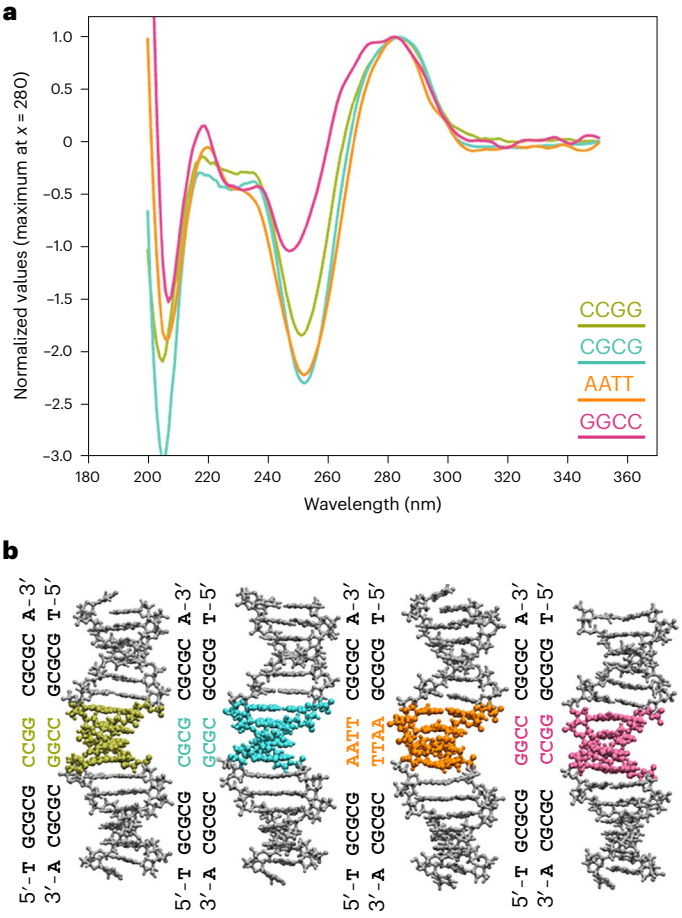

Fig. 2 | Structure and stability analysis of 16-bp sequences. a, The CD spectra of the four sequences studied. **b**, The representative structure of each sequence from the centre of the top cluster from 100 ns of MD simulation.

of current-versus-distance traces for each DNA molecule (Fig. 1b; two-dimensional (2D) conductance histogram of the CGCG molecule) and then constructed one-dimensional conductance histograms for each, as depicted in Fig. 1c. To extract the conductance values, the histograms were fitted using a Gaussian distribution. The resulting conductance values are plotted in Fig. 1d. To ensure that the measured conductance values corresponded to the binding of the DNA molecules between the junction via the thiol ends, we conducted control experiments using sequences without the thiol groups (Supplementary Fig. 1). In these control experiments, no conductance peaks were observed, confirming the importance of contact linkage when measuring the conductance through DNA molecules.

To rule out the changes in structure dominating the charge transport properties, we performed CD and MD studies on these sequences. Figure 2a displays the CD spectra for each duplex normalized to the maximum value at 280 nm. The spectra display a distinct positive peak near 280 nm and a negative peak near 250 nm. These peaks are designated as signature signals of double-stranded DNA in the B-form conformation[38].

MD simulations were also performed for each molecule. Figure 2b shows the representative structures obtained from 100-ns MD simulations via clustering for each sequence. All simulations result in stable structures (Supplementary Fig. 2) and have a B-form conformation in solution. We note that this structure may change upon pulling in the break junction system, and it has been suggested that the conductance drop in DNA stems from breaking the terminal hydrogen bonds upon pulling, which in turn disrupts the π-stack[21]. Hydrogen bonding between each base pair also provides insight into the inter-strand structural dynamics and stability of the molecules as illustrated in Supplementary Fig. 3. Furthermore, we have calculated the melting temperatures of the molecules that are presented in Supplementary Table 1, indicating that the duplexes remain stable at room temperature. Therefore, from these CD results, MD simulations and melting temperature calculations, we conclude that structural changes are not likely to be the primary factor driving the large observed conductance differences.

To understand the differences in the conductance values observed in these duplexes, we employed DFT and Green's function approaches to examine the electronic properties of the representative structures from MD[45]. These methods allowed us to determine the DoS in the oligonucleotide systems as a function of both energy and length. Since charge transport in DNA molecules is typically dominated by holes[46], we specifically focused on the region around the highest occupied molecular orbital (HOMO). Figure 3a presents 2D DoS plots for these sequences. The horizontal axis represents the spatial position of the DoS for each molecular sequence, the vertical axis shows the value of the energy levels and the colour map represents the DoS on a log scale. In this representation, specific energy levels are depicted as horizontal stripes, which inherently show their energy distribution and spatial delocalization, which we note often extends over several base pairs, as discussed previously[2,17,19]. As can be seen in Fig. 3a, below the HOMO energy, there are two regions with higher densities, creating potential 'band-like' regions, one around −5 eV and another around −6 eV, though neither are high enough density to be considered a 'band' in the conventional sense.

To see the effect of molecular structure on the DoS, we also calculated the DoS of the ideal B-form structures. The results demonstrate that, if one does not consider the overall molecular structures, the DoS values outside the bridge sequence domains do not exhibit large changes (Supplementary Fig. 4). In fact, the sequence difference within the bridge region affects the molecular structure of the whole DNA structure and, hence, the DoS of the entire molecule changes. These results emphasize the importance of molecular structure predictions via MD trajectories and clustering algorithms[38].

In the context of a hopping transport mechanism, there is a probability associated with a charge hopping into any available state in the system, which is determined by the energy difference between the occupied state and the empty state, and the coupling between them[47]. For the 2D DoS plots in Fig. 3b, we assumed that the closest state to the contact in the upper band region (Fig. 3a, black arrow) would be the most probable for initial occupation, which we refer to as the gateway state with energy E_{GS}. According to Fermi's golden rule, for the charge to travel across the molecule, it can only transition to other states that have the same energy as the initial state. Of course, the charge can relax in any given state during hopping and lose phase information. Thermal fluctuations aid this relaxation and transition process, so we examined the DoS in regions within $\pm 3k_BT$ of the gateway state for each molecular system (Fig. 3b). We also noted that the gateway state is different if the charge is entering the molecule from the left or right side; however, in either case, the analysis, discussed further below, is consistent (Supplementary Fig. 5).

Looking at this region around the gateway state (Fig. 3b), we saw that the distribution of the DoS along the DNA molecule was very different from case to case. To visualize this distribution more effectively, we plotted the cumulative number of states per unit energy and per unit volume for each base pair along the molecule (as shown in Fig. 3c and as a three-dimensional (3D) structure in Fig. 3d) within this $6k_BT$ region. The DoS for the CCGG sequence, which had the highest conductance, had a consistent distribution of states available around E_{GS}, and the states were highly delocalized throughout the molecule. This distribution promotes efficient charge transport, increasing the likelihood that the charge can effectively move through the molecule once it has entered the E_{GS} state. Similarly, the CGCG sequence has a relatively

https://doi.org/10.1038/s41557-025-01999-2

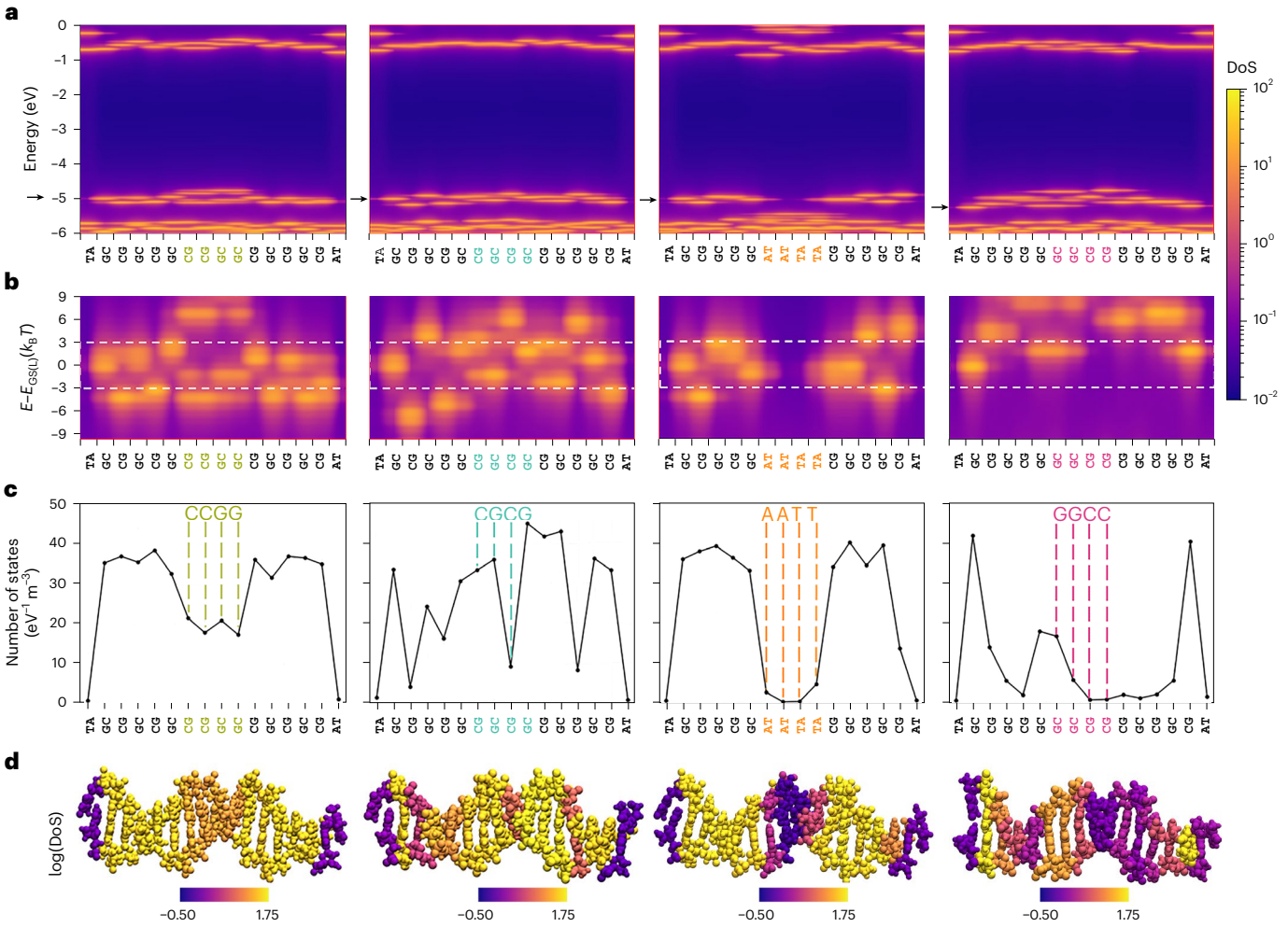

Fig. 3 | The DoS of the DNA duplexes. a, The 2D DoS for each of the molecules. The black arrows represent the energy of left gateway state, $E_{GS(L)}$, for each sequence. **b**, The 2D DoS within $\pm 9k_BT$ of $E_{GS(L)}$. The $\pm 3k_BT$ region is highlighted with dashed white boxes. **c**, The sum of states in the $\pm 3k_BT$ (total of $6k_BT$) region for all molecules. **d**, A 3D visualization of the cumulative states of the $\pm 3k_BT$ region, coloured on a log scale.

large DoS throughout this $6k_BT$ region. However, the total density is less than in the previous case; it fluctuates more as one travels across the molecule, and the states are more localized and, correspondingly, the conductance is ~10 times lower than that of CCGG. To quantify the extent of delocalization of the states, we examined the inverse participation ratio[48] for each case as a function of energy around the HOMO levels of molecules (Supplementary Fig. 6 and Supplementary Section 6).

In contrast, the AATT molecule exhibited a noticable gap in the DoS in the bridge region. However, the remaining parts of the molecule showed a near continuous density in this energy range, similar to the CCGG case. This structure suggests that the charge will tunnel through the A–T base pairs, consistent with what has been previously discussed in literature[16,33,46]. Correspondingly, the conductance of this molecule was less than either the CCGG or the CGCG sequences. However, we also noted that, despite the lack of a continuous band across the molecule, the states from the G–C pairs on either side of the AATT sequence extended well into this gap region, which, when combined with the relatively low energy barrier height (Fig. 3a) and the energy alignment between the guanines on either end of the bridge region, should allow efficient tunnelling through this barrier.

Finally, we turn to the least conductive of the four molecules, the GGCC bridge sequence, where we observed a scarcity of states within this $6k_BT$ region. In existing literature, it is widely recognized that triple G bases exhibit strong coupling with each other, leading to the delocalization of states across the three bases[17,29], which yields a splitting of the energy levels. This splitting typically manifests as a lower ionization potential than for a single G[49]. From this, one might initially assume that GGG triplets would then result in higher conductance due to these changes in delocalization and ionization potential. However, our experimental findings do not support this assumption in this particular case. The large energy level splitting in triple G bases decreased the coupling between these triplet bases and their NNBPs and expanded the DoS over a wider energy range (Fig. 3b–d). Consequently, the DoS in the vicinity around E_{GS} is greatly reduced compared with any of the other cases, even the AATT case. This lack of states limits the efficiency of charge hopping along the DNA strand because the energy fluctuations required to allow state alignment are larger, thus resulting in a considerable decrease in the overall conductance.

Preliminary design guidelines for DNA sequences

This analysis of the distribution of the DoS around E_{GS} provides valuable insights into the parameters that control coherence and transport in DNA and allows us to develop a conceptual understanding of the experimental results. From these results, we deduced a preliminary set of design guidelines that will provide a basis for designing longer sequences that maintain good charge transport properties over longer distances. In generalizing the earlier discussion, we note that: (1) long alternating G–C sequences can result in fluctuations in the DoS and a decrease in delocalization; (2) G doublets can have delocalized states

https://doi.org/10.1038/s41557-025-01999-2

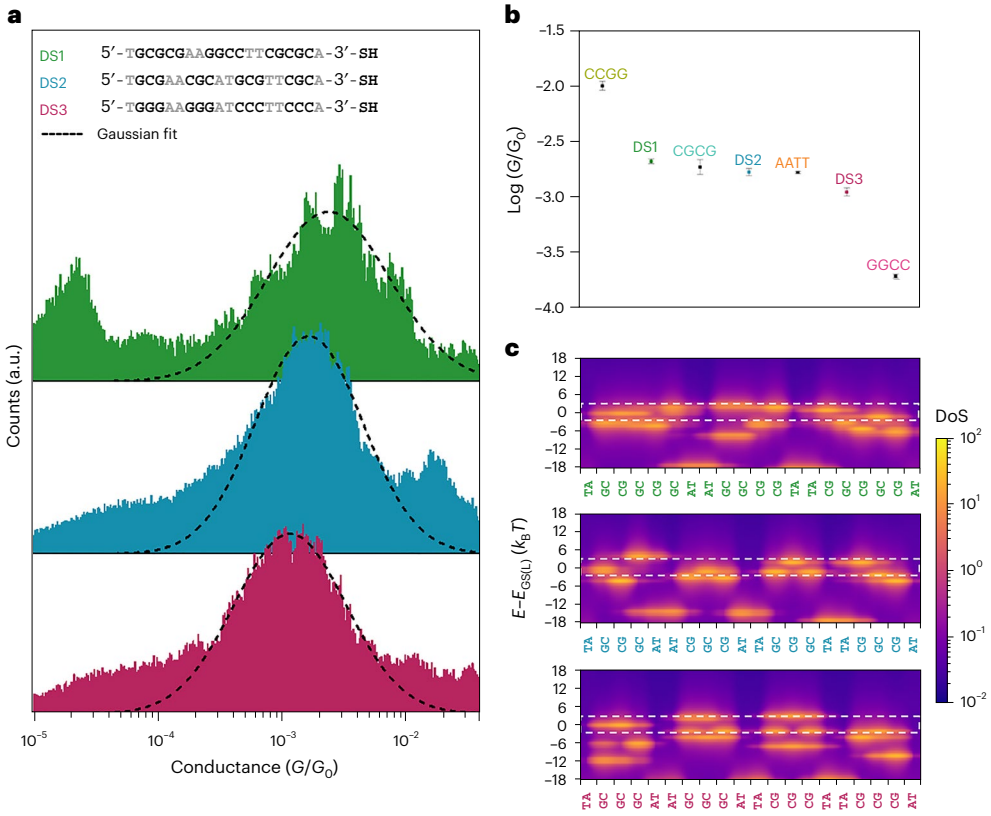

Fig. 4 | Charge transport in 20-bp sequences designed using the guidelines. **a**, Colour-coded conductance histograms of the three designed sequences. **b**, A scatter plot demonstrating the conductance values extracted from Gaussian fits for the designed 20-bp sequences and for the 16-bp sequences (5′-T GCGCG-XXXX-CGCGC A-3′). Error bars represent the standard error of the mean from four measurements. **c**, The 2D DoS of the 20-bp sequences within $\pm 18 k_B T$ of the left gateway state. The $\pm 3 k_B T$ region is highlighted with a dashed white box.

and energy splitting, but the splitting is small compared with thermal fluctuations; (3) G doublets can stabilize the DoS for G–C-rich regions, improving the overall DoS; (4) G triplets increase the energy splitting and the distribution of the DoS when combined with alternating G–C sequences; (5) A–T base pairs act as tunnel barriers; and (6) states from G–C base pairs can extend into A–T base pairs, decreasing the overall tunnelling distance.

Thus, on the basis of these observations, we aimed to design 20-bp-long self-complementary sequences that maintain high conductance values. We focused on 20-bp sequences as an initial test of the design rules, as this increase in length could easily lead to a considerable decrease in the overall conductance if the inferences about coupling were incorrect. Moreover, from a biological standpoint, longer sequences provide greater specificity for a DNA probe when interacting with its targets, opening avenues for incorporating these systems with bioanalytic processes. Finally, A–T base pairs were integrated into our designed sequence to facilitate higher purity DNA synthesis and minimize the formation of secondary structures[50].

For an initial design, we started with a system that included G doublets in the centre region and alternating G–C sequences on the ends, as this was similar to our highest conducting 16-bp sequence. However, we also included A–T base pairs to decouple the G doublets from the alternating G–C sequences, as noted previously. We hypothesized that this structure would minimize the overall impact of the tunnelling barrier on the transport while aiding in the decoupling between the centre region and the G–C supports (Fig. 4a; designed sequence 1 (DS1)). As desired, this sequence, despite being longer and having two tunnel bridges in the structure, was approximately 30% more conductive than the 16-bp AATT sequence, despite having the same number of A–T pairs, and was more than ten times more conductive than the 16-bp GGCC sequence; however, because of the inclusion of the A–T tunnel barriers, it was still lower than the 16-bp CCGG sequence. This finding further supports our hypothesis about the impact of coupling to the bridge region on charge transport across the entire molecule.

To further test the design guidelines, we added additional A–T base pairs to the sequence and used short stretches of alternating G–C sequences throughout. To do so, we moved the A–A doublets further towards the ends of the molecule and inserted an alternating A–T doublet into the middle (Fig. 4a; DS2). As verified by CD measurements, this 20-bp sequence also maintained B-form structure in a phosphate-buffered solution (Supplementary Fig. 7). Analysis of MD trajectories (root mean square deviation and hydrogen bonding) for these 20-bp sequences are given in Supplementary Figs. 8 and 9. Interestingly, the additional A–T barrier had a minimal impact on the overall conductance compared with DS1, leaving this molecule with a conductance value of $(1.67 \pm 0.13) \times 10^{-3} G_0$, which is similar to the 16-bp AATT sequence and only slightly less than the CGCG sequence. This implies that the coupling between G–C base pairs through the A–T barriers is decreased compared with the NNBP coupling in the alternating G–C cases but the tunnelling probability is high enough to maintain a reasonable conductance value.

Finally, we attempted to use these design guidelines to improve the conductance of a sequence with G triplets, while still including A–T bases in the stack. Considering that G triplets have a lower ionization potential, instead of using the alternating G–C sequences to support a G triplet bridge region, we used G triplets throughout the sequence, hypothesizing that this would improve the energy match and coupling between potential hopping sites in the system. We then proceeded to construct a sequence using G triplets, interspersed with

A–T doublets to create localized energy levels on each triplet to create design sequence 3 (DS3; Fig. 4a). This sequence yielded a conductance value of $(1.11 \pm 0.09) \times 10^{-3} G_0$, which was slightly less than the other 20-bp sequences, but an order of magnitude higher than the 16-bp GGCC sequence, suggesting that the energy matching approach drastically improved the overall transport properties. Figure 4b shows the conductance values corresponding to the peak values extracted from Gaussian fits for each molecule.

In Fig. 4c, the 2D DoS for the designed sequences within $\pm 18 k_B T$ of the gateway state for each molecule are shown. The outcomes aligned well with our proposed design guidelines and the experimental findings. The DoS plot for DS1 shows the highest density and delocalization of states within the gateway region. These states extend into the tunnelling barriers, establishing an efficient charge transport pathway, making DS1 the most conductive among the 20-bp sequences. DS2, while showing a high DoS, demonstrated less delocalization, resulting in a 20% lower conductivity compared with DS1. Lastly, DS3 DoS displayed distinct tunnelling barriers with highly split states. Despite the energy level splitting caused by GGG, there were still abundant states in the gateway region as this is also determined by a G triplet. Cumulative densities are given in Supplementary Fig. 10 and the 2D DoS plots for the right gateway region are shown in Supplementary Fig. 11.

Conclusions

This work demonstrates that consideration of charge delocalization and electronic state density is necessary to understand and control charge transport in DNA duplexes in ambient conditions, reinforcing the notion that coherence plays an important role in transport even in these warm, wet environments. We show that the coupling between NNBPs dictates the delocalization of energy levels and is a major contributing factor in determining the overall conductance of DNA molecules. Our findings add to the growing literature indicating that G–C base pairs do not function as isolated hopping sites. Rather, charge delocalization across multiple bases during transport emerges as a crucial phenomenon. The coupling between them induces notable changes in the electronic properties, as the states split, and the overall DoS becomes more dispersed. Interestingly, the sequence with the lowest ionization potential and a HOMO level nearest to the Fermi energy of the electrodes was the least conductive.

The insights gained from these observations have enabled the formulation of preliminary design guidelines that consider the effects of G singlets, doublets and triplets, as well as A–T tunnelling barriers on the overall transport properties. This work provides an initial step towards the goal of designing the system's electronic structure a priori. This enhanced comprehension of the impact of neighbouring bases and energy state delocalization on the charge transport properties of DNA, coupled with the ability to design sequences with desired properties, opens promising avenues for developing more efficient DNA nanowires. These advancements hold real potential for applications in nanoelectronics, nanofabrication and biosensing.

Online content

Any methods, additional references, Nature Portfolio reporting summaries, source data, extended data, supplementary information, acknowledgements, peer review information; details of author contributions and competing interests; and statements of data and code availability are available at https://doi.org/10.1038/s41557-025-01999-2.

References

1. Lloyd, S. Quantum coherence in biological systems. *J. Phys. Conf. Ser.* **302**, 012037 (2011).
2. Liu, C. et al. Engineering nanometre-scale coherence in soft matter. *Nat. Chem.* **8**, 941–945 (2016).
3. Liu, H. et al. Single-molecule photoelectron tunnelling spectroscopy. *Nat. Mater.* **22**, 1007–1012 (2023).
4. Venkataraman, L. et al. Single-molecule circuits with well-defined molecular conductance. *Nano Lett.* **6**, 458–462 (2006).
5. Aradhya, S. V. & Venkataraman, L. Single-molecule junctions beyond electronic transport. *Nat. Nanotechnol.* **8**, 399–410 (2013).
6. Ha, T. Q., Planje, I. J., White, J. R. G., Aragonès, A. C. & Díez-Pérez, I. Charge transport at the protein–electrode interface in the emerging field of biomolecular electronics. *Curr. Opin. Electrochem.* **28**, 100734 (2021).
7. Coropceanu, V. et al. Charge transport in organic semiconductors. *Chem. Rev.* **107**, 926–952 (2007).
8. Roy, S. et al. Direct electrical measurements on single-molecule genomic DNA using single-walled carbon nanotubes. *Nano Lett.* **8**, 26–30 (2008).
9. Slinker, J. D., Muren, N. B., Renfrew, S. E. & Barton, J. K. DNA charge transport over 34 nm. *Nat. Chem.* **3**, 228–233 (2011).
10. De Pablo, P. J. et al. Absence of dc-conductivity in λ-DNA. *Phys. Rev. Lett.* **85**, 4992–4995 (2000).
11. Endres, R. G., Cox, D. L. & Singh, R. R. P. Colloquium: the quest for high-conductance DNA. *Rev. Mod. Phys.* **76**, 195–214 (2004).
12. Kasumov, A. Y. et al. Proximity-induced superconductivity in DNA. *Science* **291**, 280–282 (2001).
13. Fink, H.-W. & Schönenberger, C. Electrical conduction through DNA molecules. *Nature* **398**, 407–410 (1999).
14. Storm, A. J., Van Noort, J., De Vries, S. & Dekker, C. Insulating behavior for DNA molecules between nanoelectrodes at the 100 nm length scale. *Appl. Phys. Lett.* **79**, 3881–3883 (2001).
15. Zhuravel, R. et al. Backbone charge transport in double-stranded DNA. *Nat. Nanotechnol.* **15**, 836–840 (2020).
16. Li, Y., Xiang, L., Palma, J. L., Asai, Y. & Tao, N. Thermoelectric effect and its dependence on molecular length and sequence in single DNA molecules. *Nat. Commun.* **7**, 11294 (2016).
17. Xiang, L. et al. Intermediate tunnelling–hopping regime in DNA charge transport. *Nat. Chem.* **7**, 221–226 (2015).
18. Muren, N. B., Olmon, E. D. & Barton, J. K. Solution, surface, and single molecule platforms for the study of DNA-mediated charge transport. *Phys. Chem. Chem. Phys.* **14**, 13754 (2012).
19. Artés, J. M., Li, Y., Qi, J., Anantram, M. P. & Hihath, J. Conformational gating of DNA conductance. *Nat. Commun.* **6**, 8870 (2015).
20. Li, Y. et al. Comparing charge transport in oligonucleotides: RNA:DNA hybrids and DNA duplexes. *J. Phys. Chem. Lett.* **7**, 1888–1894 (2016).
21. Bruot, C., Xiang, L., Palma, J. L., Li, Y. & Tao, N. Tuning the electromechanical properties of single DNA molecular junctions. *J. Am. Chem. Soc.* **137**, 13933–13937 (2015).
22. Venkatramani, R., Keinan, S., Balaeff, A. & Beratan, D. N. Nucleic acid charge transfer: black, white and gray. *Coord. Chem. Rev.* **255**, 635–648 (2011).
23. Kawai, K. & Majima, T. Hole transfer kinetics of DNA. *Acc. Chem. Res.* **46**, 2616–2625 (2013).
24. Xu, B., Zhang, P., Li, X. & Tao, N. Direct conductance measurement of single DNA molecules in aqueous solution. *Nano Lett.* **4**, 1105–1108 (2004).
25. Hihath, J., Xu, B., Zhang, P. & Tao, N. Study of single-nucleotide polymorphisms by means of electrical conductance measurements. *Proc. Natl Acad. Sci. USA* **102**, 16979–16983 (2005).
26. Guo, X., Gorodetsky, A. A., Hone, J., Barton, J. K. & Nuckolls, C. Conductivity of a single DNA duplex bridging a carbon nanotube gap. *Nat. Nanotechnol.* **3**, 163–167 (2008).
27. Xu, B. & Tao, N. J. Measurement of single-molecule resistance by repeated formation of molecular junctions. *Science* **301**, 1221–1223 (2003).
28. Hihath, J., Guo, S., Zhang, P. & Tao, N. Effects of cytosine methylation on DNA charge transport. *J. Phys. Condens. Matter* **24**, 164204 (2012).

29. Berlin, Y. A., Burin, A. L. & Ratner, M. A. Charge hopping in DNA. *J. Am. Chem. Soc.* **123**, 260–268 (2001).
30. Giese, B. Long-distance charge transport in DNA: the hopping mechanism. *Acc. Chem. Res.* **33**, 631–636 (2000).
31. Zhang, Y. et al. DNA charge transport: moving beyond 1D. *Surf. Sci.* **652**, 33–38 (2016).
32. Jortner, J., Bixon, M., Langenbacher, T. & Michel-Beyerle, M. E. Charge transfer and transport in DNA. *Proc. Natl Acad. Sci.USA* **95**, 12759–12765 (1998).
33. Li, Y., Artés, J. M. & Hihath, J. Long-range charge transport in adenine-stacked RNA:DNA hybrids. *Small* **12**, 432–437 (2016).
34. Risser, S. M., Beratan, D. N. & Meade, T. J. Electron transfer in DNA: predictions of exponential growth and decay of coupling with donor-acceptor distance. *J. Am. Chem. Soc.* **115**, 2508–2510 (1993).
35. Zhirnov, V., Zadegan, R. M., Sandhu, G. S., Church, G. M. & Hughes, W. L. Nucleic acid memory. *Nat. Mater.* **15**, 366–370 (2016).
36. Veselinovic, J. et al. Two-tiered electrical detection, purification, and identification of nucleic acids in complex media. *Electrochim. Acta* **313**, 116–121 (2019).
37. Aminiranjbar, Z. et al. Identifying SARS-CoV-2 variants using single-molecule conductance measurements. *ACS Sens.* **9**, 2888–2896 (2024).
38. Li, Y. et al. Detection and identification of genetic material via single-molecule conductance. *Nat. Nanotechnol.* **13**, 1167–1173 (2018).
39. Pattiya Arachchillage, K. G. G. et al. Electrical detection of RNA cancer biomarkers at the single-molecule level. *Sci. Rep.* **13**, 12428 (2023).
40. Conwell, E. M. Charge transport in DNA in solution: the role of polarons. *Proc. Natl Acad. Sci.USA* **102**, 8795–8799 (2005).
41. Li, L.-Y. et al. A primer design strategy for PCR amplification of GC-rich DNA sequences. *Clin. Biochem.* **44**, 692–698 (2011).
42. McDowell, D. G., Burns, N. A. & Parkes, H. C. Localised sequence regions possessing high melting temperatures prevent the amplification of a DNA mimic in competitive PCR. *Nucleic Acids Res.* **26**, 3340–3347 (1998).
43. Liu, S. et al. Direct measurement of electrical transport through G-quadruplex DNA with mechanically controllable break junction electrodes. *Angew. Chem. Int. Ed.* **49**, 3313–3316 (2010).
44. Renaud, N., Berlin, Y. A., Lewis, F. D. & Ratner, M. A. Between superexchange and hopping: an intermediate charge-transfer mechanism in poly(A)–poly(T) DNA hairpins. *J. Am. Chem. Soc.* **135**, 3953–3963 (2013).
45. Qi, J., Edirisinghe, N., Rabbani, M. G. & Anantram, M. P. Unified model for conductance through DNA with the Landauer–Büttiker formalism. *Phys. Rev. B* **87**, 085404 (2013).
46. Giese, B., Amaudrut, J., Köhler, A.-K., Spormann, M. & Wessely, S. Direct observation of hole transfer through DNA by hopping between adenine bases and by tunnelling. *Nature* **412**, 318–320 (2001).
47. Borrelli, R., Capobianco, A. & Peluso, A. Hole hopping rates in single strand oligonucleotides. *Chem. Phys.* **440**, 25–30 (2014).
48. Adjizian, J.-J., Lherbier, A. M.-M., Dubois, S., Botello-Méndez, A. R. & Charlier, J.-C. The electronic and transport properties of two-dimensional conjugated polymer networks including disorder. *Nanoscale* **8**, 1642–1651 (2016).
49. Di Felice, R., Calzolari, A., Molinari, E. & Garbesi, A. Ab initio study of model guanine assemblies: the role of π–π coupling and band transport. *Phys. Rev. B* **65**, 045104 (2001).
50. Keel, A. Y., Easton, L. E., Lukavsky, P. J. & Kieft, J. S. Large-Scale Native Preparation of In Vitro Transcribed RNA. in *Methods in Enzymology* vol. 469 (ed Herschlag, D.) 3–25 (Elsevier, 2009).

Methods

Sample preparation

Single stranded DNA molecules were purchased from Alpha DNA at 1 µmole scale, where they were purified using high-performance liquid chromatography. The 3′ ends were modified with three-carbon chains and thiol linkers. The molecules were treated with dithiothreitol to reduce the thiols, and the excess dithiothreitol was then removed using ethanol precipitation and lyophilized. The molecules were resuspended using nuclease-free water purchased from Thermo Fisher. To prevent any degradation, all samples were stored at −80 °C. The working solutions were prepared using a 100 mM phosphate buffer solution mixed with DNA molecules. The buffer was prepared by combining Na_2HPO_4 and NaH_2PO_4 (Sigma–Aldrich) in an 8.1:1.9 volume:volume ratio at pH 7.4. To form DNA duplexes, the mixture was heated to 90 °C in a thermocycler and gradually cooled to room temperature over several hours. Glassware and Teflon sample cells used in sample preparation and during experiments were meticulously cleaned using a piranha solution (98% H_2SO_4 and 30% H_2O_2 in a 3:1 volume:volume ratio).

STM-BJ technique

All experimental procedures were conducted using a Molecular Imaging Pico-STM head. This head was connected to a modified Digital Instruments Nanoscope IIIa controller within a chamber that was both acoustically and mechanically isolated and maintained at room temperature. A LabView program and a National Instruments PCIe-6363 DAQ controlled the movement of the STM tip throughout the measurements. A 10 nA V^{-1} amplifier was utilized in the experiments. In each experiment, the initial step involved adding phosphate buffer to a Teflon cell positioned on top of a gold substrate. An STM tip, created from a 0.25-mm gold wire cut and coated with Apiezon wax, was immersed in the buffer solution. The tip was maintained at the tunnelling distance from the substrate before starting to tap. The data obtained in the buffer served as control experiments to ensure the absence of contaminants before each experimental run. Subsequently, double-stranded DNA molecules were introduced into the cell with a final concentration between 5 and 10 µM.

During the break junction experiment, the gold tip was brought into close proximity (tunnelling range) with the substrate within the solution containing the molecule of interest. A bias ranging from 30 to 200 mV was applied between the gold tip and substrate. The tip approached the substrate and, upon reaching a maximum current set point, the amplifier saturated, causing the tip to retract from the substrate. This retraction continued until a minimum current was reached, corresponding to the lower end of the amplifier, at around 10 pA. This lower limit may cause an additional peak in the conductance histogram at low conductance values, as seen in Fig. 4a in the histogram for DS1. This cycle was repeated 3,000–5,000 times for each set of experimental parameters (bias, pulling rate, etc.), and the current-versus-distance traces were recorded. Occasionally, during the retraction phase, a molecule binds between the tip and substrate, resulting in a plateau (step) in the current traces. To obtain statistical values, the collected data were processed using a LabView program developed in the laboratory. The analysis uses a linear fit for each current trace in a semi-log scale. Traces with a residual sum of squares below a set criterion (for example, 0.4) are rejected by the program, allowing for the separation of data depicting a step versus those with only a logarithmic decay. The selected current traces were then used to build the conductance histogram, displaying the conductance peak representing the most probable conductance of the molecule in the solution. In these experiments between 20% and 35% of the traces had a conductance plateau. For each of the conductance values reported, at least four independent experiments were performed, with a conductance yield of >20% per experiment to obtain the average conductance values. An *I*–*V* curve for a 16-bp sequence bridged with CGCG is given in Supplementary Fig. 12 as an example.

CD

CD experiments were performed using an Olis RSM 1000 circular dichromator with a cylindrical cell (170 µl) and 0.1 mm path length. Before every CD measurement, a blank spectrum, using only the buffer solution, was collected and then subtracted from the experimental data. A 170 µl volume of 50 µM double-stranded DNA in phosphate buffer was added to the cell. CD spectra (absorbance intensity versus wavelength) at 21 °C were plotted and smoothed using the adjacent averaging method with a 10-point window.

MD simulations

The initial DNA double-strand 3D structure coordinates were generated using AMBER Nucleic Acid Builder[51] for 16-bp and 20-bp DNA sequences. All DNA structures were neutralized with Na^+ counter ions (30 Na^+ ions for 16-bp DNAs and 38 Na^+ ions for 20-bp DNAs) and solved with TIP3P[52] water molecules with a 15 Å cutoff barrier from all boundaries in an octahedral periodic simulation box. To parameterize DNA structures, the bsc1[53] force field was used. For all DNA structures, the same minimization, heating, equilibration and production steps were applied using the AMBER16[51] software pmemd.cuda module; the steps are given in detail below.

First, water molecules and Na^+ counter ions were minimized with 500 steps using the steepest descent method, followed by 500 steps of conjugate gradient minimization while a 25 kcal mol^{-1} restraint force was applied to the DNA structure. The whole system, including water, ions and DNA structure, was minimized with 1,000 steps of steepest descent and 1,000 steps of the conjugate gradient method, respectively. Then, the system was heated to 300 K with a 3 K ps^{-1} heating rate while keeping the DNA structure under the 25 kcal mol^{-1} restraint force in the *NVT* ensemble. Next, the system was equilibrated for 100 ps with a 0.5 kcal mol^{-1} restraint force on the DNA structure in the *NPT* ensemble. Finally, the whole system was equilibrated for another 2.5 ns without any restraints on the DNA. This was then followed by a 100-ns MD simulation in the *NPT* ensemble. The time step used for these MD simulations (2.5 ns equilibration and 100 ns production) was set to 2 fs and the SHAKE[54] algorithm was applied to constrain all bonds to hydrogen. Lastly long-range electrostatic interactions were modelled using the Particle-Mesh Ewald[55] method with a 10 Å cutoff for van der Waals interactions.

Choosing representative structures from MD trajectories

A root mean square deviation-based structural clustering algorithm was used to group all of the structures acquired by MD simulations using VMD software[56]. Cutoff values of 2.00 Å and 2.25 Å were chosen to cluster the 16-bp and 20-bp DNA structures, respectively. We then selected the centroid structures from the most populated clusters for each sequence to evaluate the electronic properties. Subsequently, the geometry of structures was optimized with energy minimization to relax residual strains. Then, the minimized structures were used in the first principle calculations.

DFT and DoS calculations

To perform DFT, Na^+ counter ions and water molecules were removed from the minimized representative structures. The total charge of the system was set to −30 and −38 for 16-bp and 20-bp DNA structures, respectively. DFT calculations were carried out using Gaussian 09 (ref. 57) software with the B3LYP exchange–correlation function and the 6-31G(d,p) basis set. The self-consistent reaction field was set to water using the integral equation formalism polarizable continuum model[58] and solvation model density[59], which applies the integral equation formalism polarizable continuum model protocol with Coulomb radii and non-electrostatic contributions for 16-bp and 20-bp DNA molecules, respectively.

We then obtained Fock (*F*) and overlap (*S*) matrices from the DFT calculations and employed a Löwdin transformation to convert Fock

and overlap matrices into a Hamiltonian (H_o) in an orthogonal basis set by

$$H_o = S^{-\frac{1}{2}} F S^{-\frac{1}{2}} \quad (1)$$

and apply a unitary (U) transformation to transform the Hamiltonian matrix into a block diagonal matrix, H, using equation (2)

$$H = U^{\dagger} H_o U \quad (2)$$

Here, † represents the conjugate transpose. The diagonal elements of the block diagonal Hamiltonian matrix represent the energy levels of each atomic orbital, while off-diagonal elements account for coupling between atomic orbitals.

The DoS along the atoms of the molecule in each energy is calculated by finding retarded Green's function (G^r) method as follows:

$$[E - (H + \Sigma_L + \Sigma_R + \Sigma_B)]G^r = I \quad (3)$$

where H is the Hamiltonian matrix, E is energy and I is the identity matrix with the same size as H. $\Sigma_{L,R}$ describe the self-energies of left and right contact and Σ_B is the self-energy of the decoherence (Büttiker) probe. Finally, the DoS of each atom in each energy level can be calculated using the following equation:

$$\mathrm{DoS}(m, E) = -\frac{\mathrm{Im}[\mathrm{diag}(G^r_m(E))]}{\pi} \quad (4)$$

To acquire 2D DoS plots, we summed the DoS values of each atom for the corresponding base pair at each energy level, including the backbone and base atoms of the base pair.

Data availability

Data that support the findings of this study are available within the paper and its Supplementary Information. Source data are provided with this paper.

References

51. Case, D. A. et al. AMBER16 (University of California, San Francisco, 2016).
52. Jorgensen, W. L., Chandrasekhar, J., Madura, J. D., Impey, R. W. & Klein, M. L. Comparison of simple potential functions for simulating liquid water. *J. Chem. Phys.* **79**, 926–935 (1983).
53. Ivani, I. et al. Parmbsc1: a refined force field for DNA simulations. *Nat. Methods* **13**, 55–58 (2016).
54. Miyamoto, S. & Kollman, P. A. Settle: an analytical version of the SHAKE and RATTLE algorithm for rigid water models. *J. Comput. Chem.* **13**, 952–962 (1992).
55. Darden, T., York, D. & Pedersen, L. Particle mesh Ewald: an *N*·log(*N*) method for Ewald sums in large systems. *J. Chem. Phys.* **98**, 10089–10092 (1993).
56. Humphrey, W., Dalke, A. & Schulten, K. VMD: visual molecular dynamics. *J. Mol. Graph.* **14**, 33–38 (1996).
57. Frisch, M. J. Gaussian 09 (Gaussian Inc., 2009).
58. Scalmani, G. & Frisch, M. J. Continuous surface charge polarizable continuum models of solvation. I. General formalism. *J. Chem. Phys.* **132**, 114110 (2010).
59. Marenich, A. V., Cramer, C. J. & Truhlar, D. G. Universal solvation model based on solute electron density and on a continuum model of the solvent defined by the bulk dielectric constant and atomic surface tensions. *J. Phys. Chem. B* **113**, 6378–6396 (2009).

Acknowledgements

The authors acknowledge funding support from the National Science Foundation Growing Convergence and Future Manufacturing Programmes, grant no. NSF-2317843/2328217 (to J.H.). The numerical calculations reported in this paper were partially performed at TUBITAK ULAKBIM, High Performance and Grid Computing Center (TRUBA resources; E.E.O.). We thank M. P. Anantram and A. De for fruitful and enlightening discussions.

Author contributions

Z.A. performed experiments and analysed the data. A.Z. aided in the CD experiments. C.A.G. performed the modelling and simulation studies. E.E.O. supervised the modelling efforts. J.H. conceived the idea and supervised the experiments. All authors aided in drafting the manuscript.

Competing interests

The authors declare no competing interests.

Additional information

Supplementary information The online version contains supplementary material available at https://doi.org/10.1038/s41557-025-01999-2.

Correspondence and requests for materials should be addressed to Ersin Emre Oren or Joshua Hihath.

Peer review information *Nature Chemistry* thanks Julio Palma, Danny Porath and the other, anonymous, reviewer(s) for their contribution to the peer review of this work.